Research article

A potential biological signature of 7-methylguanosine-related lncRNA to predict the immunotherapy effects in bladder cancer

Shangxun Xie [a,1], Jibao He [b,1], Baofu Feng [c], Dapang Rao [a], Shuaibin Wang [a], Youhua He [a,*]

[a] Department of Urology, The Second Affiliated Hospital and Yuying Children's Hospital of Wenzhou Medical University, Wenzhou, Zhejiang Province 325000, People's Republic of China
[b] Department of Urology, Jiangsu Province Academy of Traditional Chinese Medicine, Nanjing, Jiangsu Province 210028, People's Republic of China
[c] Nanjing Medical University, Nanjing, Jiangsu Province 210028, People's Republic of China

ARTICLE INFO

ABSTRACT

Background: Bladder urothelial carcinoma (BLCA) is the second prevalent genitourinary carcinoma globally. N7-methylguanosine (m7G) is important for tumorigenesis and progression. This study aimed to build a predictive model for m7G-related long non-coding RNAs (lncRNAs), elucidate their role in the tumor immune microenvironment (TIME), and predict immunotherapy response in BLCA.
Methods: We first used univariate Cox regression and coexpression analyses to identify m7G-related lncRNAs. Next, the prognostic model was built by utilizing LASSO regression analysis. Then, the prognostic significance of the model was examined utilizing Kaplan-Meier survival analysis, receiver operating characteristic (ROC) curves, nomogram, and univariate, multivariate Cox regression. We also analyzed Gene set enrichment analyses (GSEA), immune analysis and principal component analysis (PCA) in risk groups. To further predict immunotherapy effectiveness, we evaluated the predictive ability for immunotherapy in 2 risk groups and clusters using tumor immune dysfunction and exclusion (TIDE) score and Immunophenoscore (IPS).
Results: Seven lncRNAs related to m7G were used to create a model. The calibration plots for the model suggested a strong fit with the prediction of overall survival (OS). The area under the curve (AUC) for first, second, and third years was respectively, 0.722, 0.711, and 0.686. In addition, the risk score had strong correlation with TIME features and genes linked to immune checkpoint blockade (ICB). TIDE scores were dramatically different between two risk groups (p < 0.05), and IPS scores were markedly different between two clusters (p < 0.05).
Conclusion: Our research constructed a novel m7G-related lncRNAs that could be used to predict patient outcomes and the effectiveness of immunotherapy in BLCA. Immunotherapy may be more effective for the low-risk group and cluster 2.

1. Introduction

With 549,000 new cases and 200,000 fatalities globally from bladder cancer in 2018, bladder urothelial carcinoma (BLCA) is the

---

* Corresponding author.
  E-mail address: heyouhua304@163.com (Y. He).
[1] Shangxun Xie and Jibao He contributed equally to this work.

Abbreviations

BLCA	Bladder urothelial carcinoma
m7G	N7-Methylguanosine
TICs	Tumor-infiltrating immune cells
ROC	Receiver operating characteristic
TIME	Tumor immune microenvironment
PCA	Principal component analysis
KEGG	Kyoto Encyclopedia of Genes and Genomes
GSEA	Gene-set enrichment analysis
TIDE	Tumor immune dysfunction and exclusion
IPS	Immunophenoscore
AUC	Area under the curve
tRNAs	Transfer RNAs
lncRNAs	Long noncoding RNAs
TCGA	The Cancer Genome Atlas
t-SNE	T-distributed stochastic neighbor embedding
PD-1	Programmed cell death-1
CTLA-4	Cytotoxic T-lymphocyte antigen 4
PD-L1	Programmed death ligand 1
PD-L2	Programmed death ligand 2
ICI	Immune checkpoint inhibitor
FC	Fold change
FDR	False discovery rate
ICB	Immune checkpoint blockade.

second most common malignant tumor of the urinary tract [1]. Effective treatment methods for bladder cancer include transurethral resection and intravesical Bacillus Calmette-Guerin for non-muscle-invasive bladder cancer, and neoadjuvant chemotherapy combined with radical cystectomy for muscle-invasive bladder cancer. Besides, recent new developments in the molecular biology and genetics of BLCA have encouraged the development of immune checkpoint inhibitor therapy and targeted therapy [2]. Because of its high overall mutation rate, bladder cancer can benefit from immunotherapy [3], especially when using checkpoint inhibitors that primarily target programmed cell death-1 (PD-1) and its receptor (PD-L1). Cancer cells can use checkpoint pathways, which are endogenous systems that control autoimmunity, to damage the immune system [4]. However, the objective response rates (15%–24%) in various clinical trials to immunotherapy were different and unsatisfactory [5,6], indicating that it was urgently necessary to identify the precise predictor of how a particular cancer would respond to immunotherapy or tumor would evolve.

Recent advances in epitranscriptomics have identified more than 170 different forms of post-transcriptional ribonucleic acid (RNA) modifications which can influence the function and metabolism of eukaryotic RNA [7]. Transfer RNAs (tRNAs) acquire diverse modifications for their structure, function, and protein synthesis [8–10]. One of the most prevalent tRNA modifications observed in prokaryotes and eukaryotes is N7-methylguanosine at position 46 (m^7G46) [11]. m7G modification of tRNAs is mediated by METTL1-WDR4 to maintain its stability [12]. Existing evidences have revealed that m7G editing is important for inhibiting cancer cell migration, including lung cancer [13] and colon cancer [14]. In contrast, METTL1-mediated m7G can promote the progression of bladder cancer by altering EGFR/EFEMP1 expression [15]. Nevertheless, the association of m7G modification with immune response and cancer development stays unclear in bladder cancer.

Long noncoding RNAs (lncRNAs) are considered to exert a vital role in modulating the gene expression that controls cell growth, differentiation, migration, and survival [16,17]. It has been demonstrated that the cancer-related processes of urological malignancies, including prostate, bladder, and kidney cancer, were significantly influenced by the dysregulated expression of lncRNAs [18]. For example, it has been discovered that the lncRNA CASC11 stimulated cell growth through inhibiting miRNA-150 expression in BLCA cell lines [19]. Moreover, BLCA cell-secreted exosomal lncRNA LNMAT2-mediated Prospero homeobox 1 activation in human lymphatic endothelial cells was promoting lymphangiogenesis and lymph node metastasis [20]. Recently, it has been demonstrated that lncRNA NEAT1′ stability was maintained by arsenic resistance protein 2, a factor that interacted with the cap-binding complex which integrated with RNA polymerase II transcripts' m7G cap structure [21]. Meanwhile, according to research, NEAT1 increased the level of HMGB1 by sponging miR-410, which promoted the development of BLCA [22]. However, the function of m7G editing on the dysregulated lncRNAs in bladder cancer is still unknown.

2. Materials and methods

2.1. Datasets collection

For subsequent study, The Cancer Genome Atlas (TCGA) database (https://portal.gdc.cancer.gov)was used to gather the

transcriptome profiling and relevant clinical data of the BLCA patients for subsequent analysis. A flow diagram summarizing the analytical procedure was displayed in Fig. 1. We eliminated BLCA patients who had missing overall survival (OS) data in order to lessen bias in our analysis. We collected 403 patients with pertinent clinical data and randomly assigned them to the train set and test set using the R package caret and Strawberry Perl. Institutional Review Board approval was not required because this is a bioinformatics article and the data originates from public source.

2.2. Selection of genes and lncRNAs related to m7G

26 m7G genes are included in the gene sets M26714, M26066, and M18244 that were retrieved from the Gene Set Enrichment Analysis (GSEA) database (http://www.gsea-msigdb.org/gsea/index.jsp) in 2021.12.30. Furthermore, with previous research about m7G [23], we acquired the profile of 29 genes related to m7G at all (Appendix Table S1). Then a correlation analysis between 29 m7G-related genes and lncRNAs was carried out. We screened 768 m7G-relatedu lncRNAs (Pearson correlation coefficients >0.4, and $p < 0.001$) through "limma" R package. Next, in order to visualize the network between m7G genes and lncRNAs, we used R package "igraph".

2.3. Construction and verification of the risk model

Firstly, we identified 452 m7G-lncRNAs that were differently expressed (Log2 fold change (FC) > 1, false discovery rate (FDR) < 0.05) through R package "limma". Univariate Cox regression analysis was utilized to detect prognosis-related lncRNAs on the basis of clinical data from TCGA. Then, 1000 cycles of Lasso regression were executed with a 0.05 p-value, along with 10-fold cross-validation and 1000 random stimulation to avoid overfitting. Next, multivariate Cox regression was employed to detect lncRNAs with the greatest prognostic significance. Secondly, the risk scores were generated in accordance with each m7G-lncRNA related to overall survival (OS) and the equation for calculating the risk score is as follows: risk score = coef-lncRNA-1 × exp-lncRNA-1+ coef-lncRNA-2 × exp-lncRNA-2 + ⋯ + coef-lncRNA-n × exp-lncRNA-n (exp means the m7G-lncRNAs' levels of expression, coef means the coefficient of prognosis-related m7G-lncRNAs). Subsequently, depending on the median risk score, we separated the patients into low- and high subgroups. Finally, Kaplan–Meier survival curves of two groups, stratified survival curves according to clinical features, and 1/2/3-year OS receiver operating characteristic (ROC) curves were constructed to assess the prognostic effect of the constructed model. Additionally, using univariate and multivariate Cox regression, it was determined if the risk score could act as a meaningful predictor of OS.
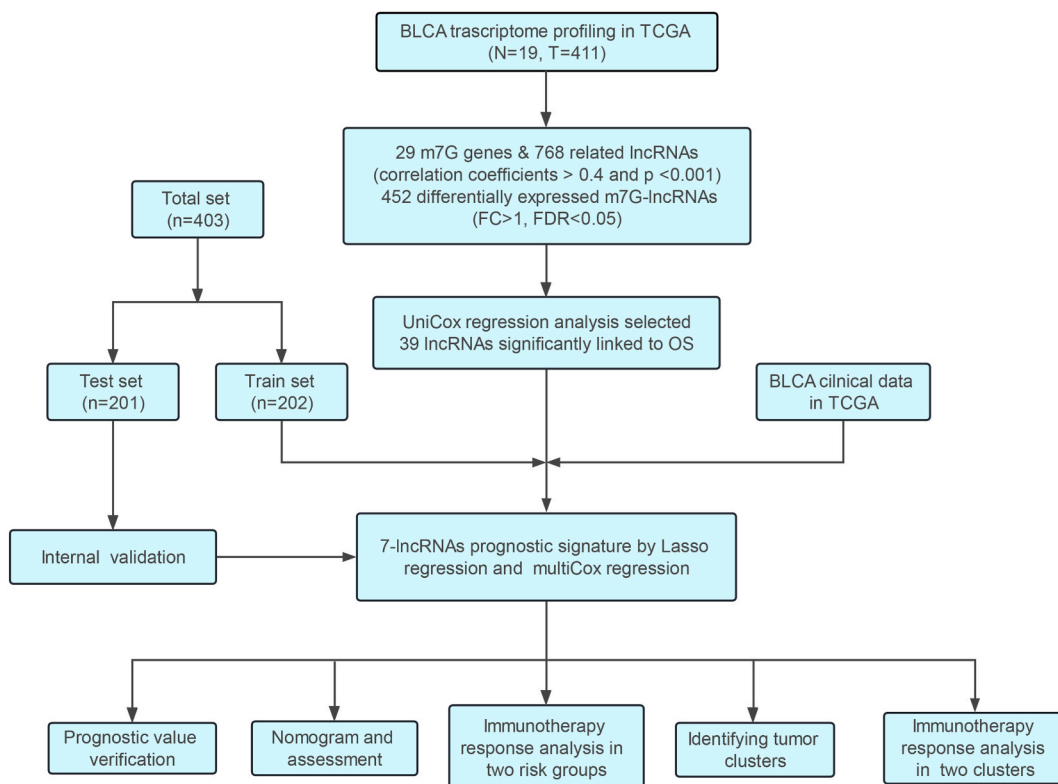

Fig. 1. The flow diagram of study.

2.4. Construction of prognostic nomogram

To estimate 1-, 2-and 3-year OS probability of patients with BLCA, a prognostic nomogram incorporating risk score, tumor stage, and age was established. Besides, the calibration curve was created to test the prognostic value of the nomogram. If the calibration curve is close to 45°, the model created using the above factors has a fair amount of predictive power.

2.5. Gene set enrichment analyses

Kyoto Encyclopedia of Genes and Genomes (KEGG) pathways enrichment analysis was applied by employing the GSEA software 4.2.2. Between the low-risk and high-risk groups, enriched pathways ($p < 0.05$ and FDR <0.25) were identified.

2.6. Relationship of risk score with tumor infiltrating immune cells characterization and immune checkpoint

Firstly, we evaluated tumor purity, the extent and concentration of stromal cells, and immune cells in two subgroups utilizing the R package "ESTIMATE". Secondly, between the low- and high-risk group, we compared tumor microenvironment (TME) signatures. Secondly, the fraction of infiltrating immune cells for each bladder cancer tissue was examined using TIMER, XCELL, EPIC, QUAN-TISEQ, MCPCOUNTER, CIBERSORT and CIBERSORT-ABS on TIMER2.0. Each immune cell type's differences between two subgroups were analyzed, as well as the relationships between the diverse immune cells and risk scores. Thirdly, using the R package "GSEAbase," a single sample gene-set enrichment analysis (ssGSEA) was conducted, and the difference of enrichment in 29 immune function-related gene sets between two subgroups was revealed. Lastly, the levels of gene expression for 47 genes associated to immune checkpoint blockade (ICB), such as CD274 and others, were also compared across the two risk groups.

2.7. Consensus clustering of bladder cancer

According to prognostic m7G-lncRNA expression, the underlying molecular clusters were investigated by using the R package "ConsensusClusterPlus". Afterward, the "Rtsne" package for R was employed to construct principal component analyses (PCA) and T-distributed stochastic neighbor embedding (t-SNE). Comparative analysis was carried out between the BLCA clusters for differences in OS, immune cell infiltration, TME, and immunological checkpoint.

2.8. Analysis of immunotherapy predictive efficacy

To explore the prediction accuracy of this model for immunotherapy in BLCA patients, we compared tumor immune dysfunction and exclusion (TIDE) score in two risk groups and two clusters through the Wilcoxon test. On TIDE website (http://tide.dfci.harvard.edu), the score was calculated. Immunophenoscore (IPS) has been proven that it can forecast the curative effect of immune checkpoint inhibitors (ICIs) [24], whose scores are based on the expression of four major components, including effector cells, MHC molecules, immunosuppressive cells, and immunomodulators. Additionally, the IPS score was calculated using a standard 0 to 10 scale for gene expression in cell types. The Cancer Immunome Atlas (TCIA) (https://tcia.at/home) was used to download IPSs for each BLCA patient.
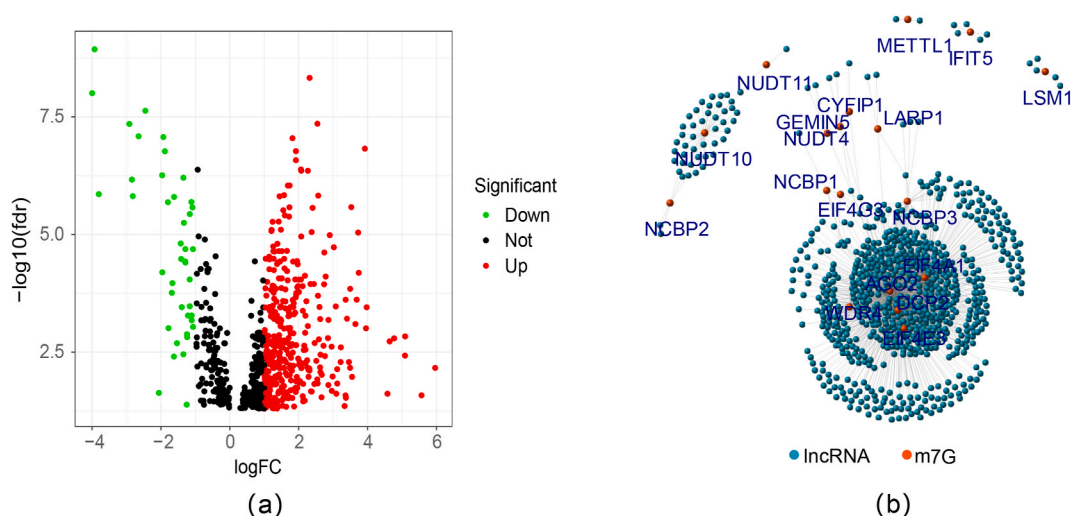

Fig. 2. Identification of m7G-related lncRNAs in patients with BLCA. (a) Volcano map of 768 differentially expressed m7G lncRNAs. (b)The network between m7G genes and lncRNAs (correlation coefficients >0.4 and p < 0.001).

3. Results

3.1. M7G-related lncRNAs in BLCA patients

The TCGA database was applied to obtain 411 tumor samples and 19 normal samples. After selecting all lncRNAs from TCGA matrix and implementing coexpression analysis with 29 m7G genes to obtain lncRNAs correlated to m7G (coefficients>0.4 and p < 0.001), to display the correlations between m7G genes and m7G-lncRNAs, an interactive network figure was created (Fig. 2b and Appendix Table S2). Next, 452 m7G-lncRNAs that showed differential expression were discovered (log2FC > 1 and p < 0.05). We found that 410 m7G-lncRNAs were upregulated, while 42 were downregulate, which was delineated in a volcano map (Fig. 2a).

3.2. Construction and confirmation of the model

39 m7G-lncRNAs linked with survival were found after the univariate Cox regression analysis and displayed on a heat map and a forest map (Fig. 3a and b). When the initial value of Log (λ) was the least deviation feasible and to prevent over-fitting of the signature, we used LASSO regression and multivariate Cox regression analysis to create 7 prognosis-related m7G-lncRNAs. The formula that was utilized to determine risk score was as followed: Risk score = AC093620.1 × (0.4532) +AC073534.2 × (−0.7682) + KCNQ1OT1 × (1.9381) + NRIR × (−0.5780) + AC083906.3 × (0.7011) + UBE2Q1-AS1 × (−1.2694) + AC253576.2 × (−0.5887).

Patients diagnosed with BLCA were separated as either low- or high-risk based on their median risk score. The allocations of survival status (Fig. 4a–c), risk score (Fig. 4d–f) and expression level (Fig. 4g–i) revealed that the prognosis was better for low-risk
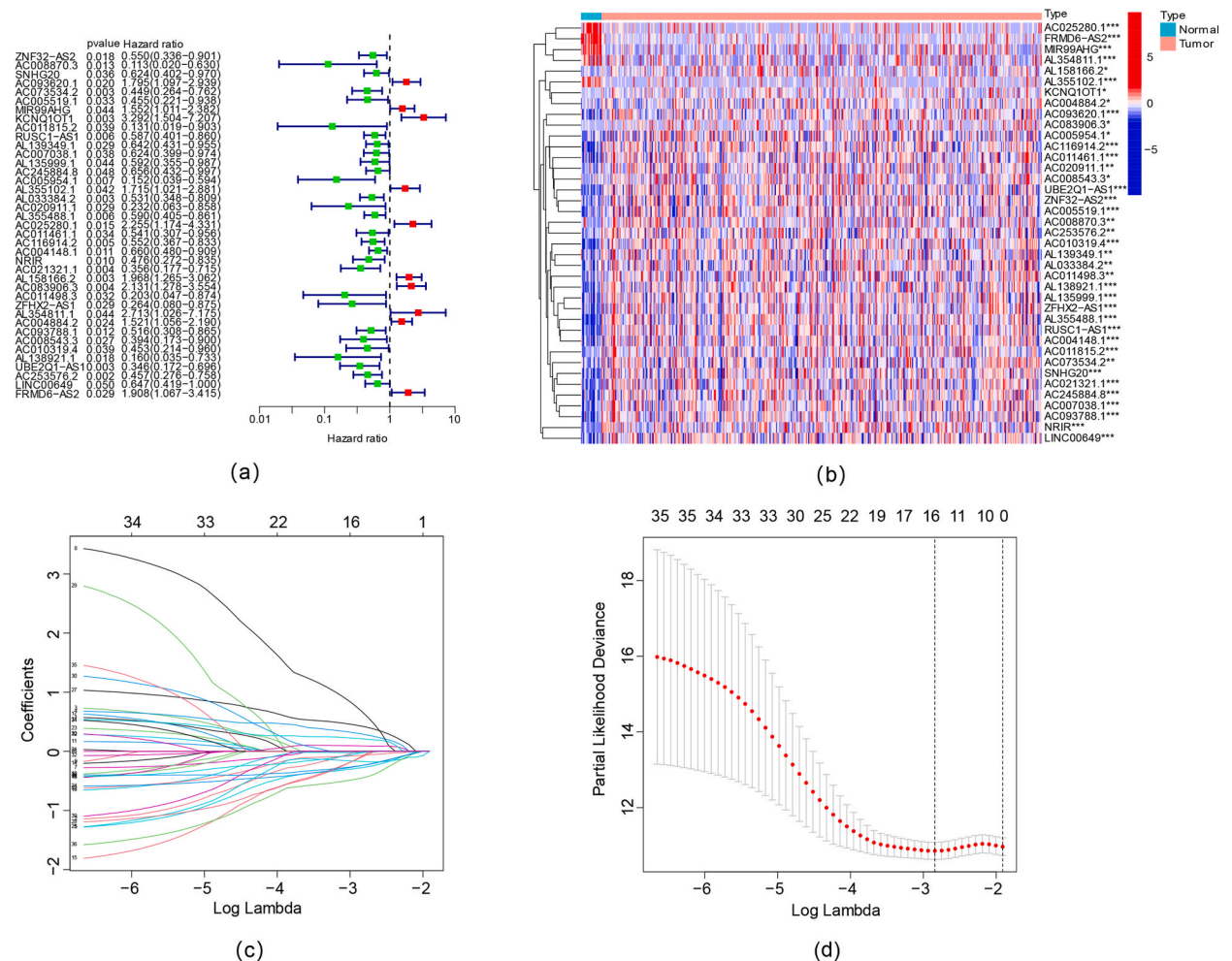

(a)

(b)

(c)

(d)

Fig. 3. Extraction of m7G-related lncRNAs prognostic markers in BLCA. (a) The prognostic m7G-lncRNAs extracted by univariate Cox regression analysis. (b) Heatmap of 39 prognostic lncRNAs expression. The expression level was compared by the Wilcoxon test (*, P < 0.05; **, P < 0.01, ***P < 0.001). (c) The 10-time cross-validation for variable selection in the lasso regression. (d) The LASSO coefficient profile of 16 m7G-related lncRNAs.

BLCA patients than for high-risk ones. Additionally, patients with high-risk features had significantly shorter OS, as seen by the Kaplan-Meier curve, compared to those with low-risk characteristics (Fig. 5a–c). Besides, the stratification survival curves according to different clinical factors (age, gender and stage) performed the same conclusion (Fig. 5d).

According to the findings of the univariate (Fig. 6a) and multivariate (Fig. 6b) Cox regression analyses, the risk score was one of the independent predictors in the overall survival of BLCA patients. Next, the nomogram was created to forecast the prognosis of BLCA patients using the risk score, age, and stage (Fig. 6c). Calibrate curves were closed to diagonal, suggesting our nomogram had a strong predictive effect for OS (Fig. 6d). Lastly, gender, age, grade, and stage were taken out as the potential prognostic predictors in order to see if risk score was a stronger prognostic predictor than other clinical parameters. The 1-year ROC curve of merged clinical variables was generated, as well as 1-, 2-, and 3-year ROC curve of risk model (Fig. 6e and f). Then we observed that risk score achieved the best AUC value.

3.3. GSEA

GSEA software was adopted to examine KEGG pathway in the whole set. Each risk group's top five pathways were displayed (Fig. 7a). We can see that melanoma pathway was significant in the high-risk group (all $p < 0.05$; FDR <0.25; $|NES| > 1.5$).

3.4. TME, immune checkpoint, and immunotherapy response in risk groups

Risk score was correlated with immunity score (derived using the ESTIMATE algorithm), tumor-infiltrating immune cells (TICs) from 7 different platforms, and ssGSEA signatures in order to further investigate if risk score may be used as immunological indicators. Firstly, we could find that the majority of immune cells presented a positive correlation with risk sores at bubble chart ($p < 0.05$), such as macrophage, myeloid dendritic cells, CD8$^+$ T cell, and neutrophil at TIMER (Fig. 7b and c and Appendix Table S3). Likewise, in the high-risk group, there was a rise in the number of every type of immune cell and immune-associated function, according to ssGSEA analysis ($p < 0.05$). (Fig. 7d and e). Secondly, 19 of 47 immune checkpoint-related genes had significantly greater expression levels in individuals with high-risk score, such as CD80, CD86, and PDCD1LG2 (PD-L2) ($p < 0.05$) (Fig. 7f). Thirdly, high-risk subgroup obtained the greater immunological score, stromal score and estimation score ($p < 0.05$) (Fig. 7g).

Afterward, TIDE was implemented to assess the immunotherapy's underlying clinical effectiveness in various risk groupings. Patients with lower TIDE scores may have less immunological escape potential, and hence may respond better from ICI therapy. According to the findings of our study, low-risk patients may benefit more from ICI treatment than high-risk patients since they had a lower TIDE score than the high-risk grouping. Additionally, microsatellite instability (MSI) was higher in the low-risk grouping, while T-cell dysfunction scores was higher in the high-risk grouping. Besides, there was no statistically significant distinction in T-cell exclusion between the two subgroups (Fig. 9a). Then, four subtypes of IPS values were utilized to reflect the responses to
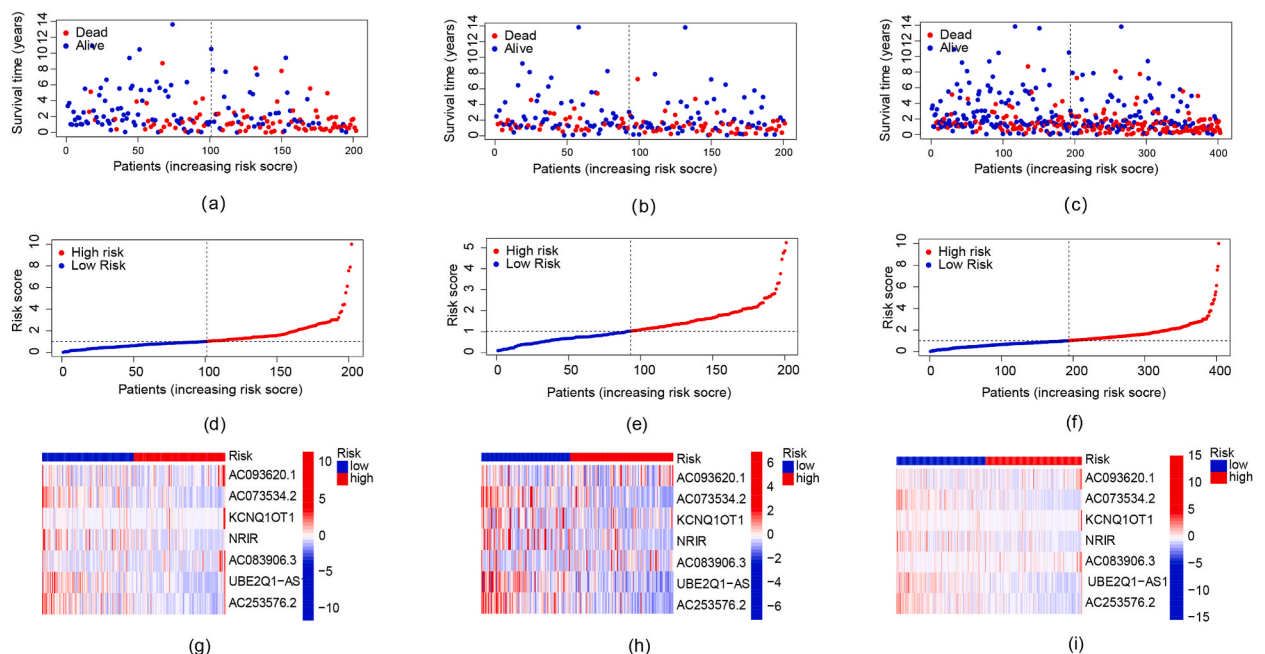

Fig. 4. Prognosis features of the 7 m7G-related lncRNAs model. (a–c) Survival status and time between low-/high-risk groups in the train, test, and whole groups. (d–f) Distribution of m7G-related lncRNAs model based on risk score of the train, test, and whole groups. (g–i) Heatmap of 7 lncRNAs expression in the train, test, and whole groups.
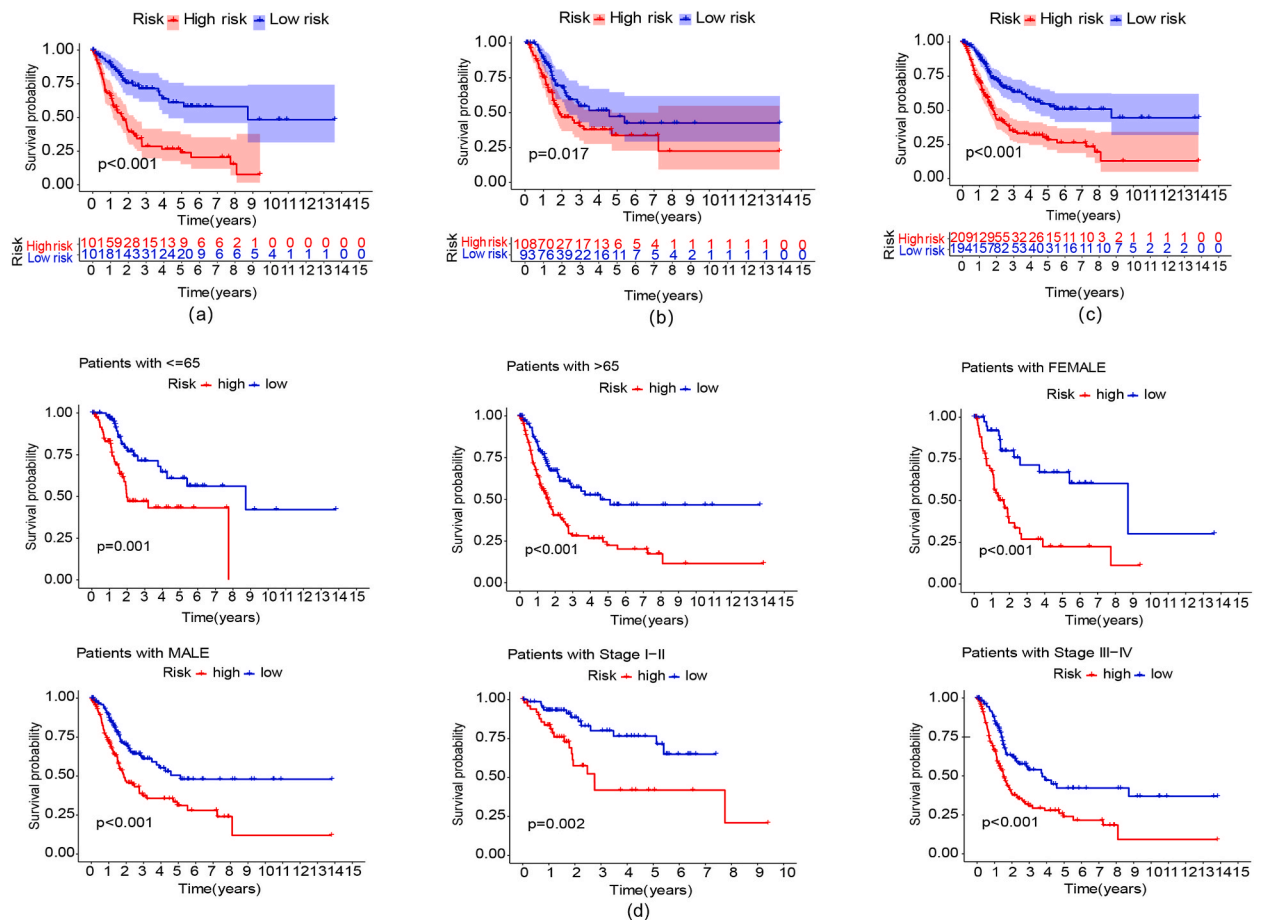
Fig. 5. Kaplan–Meier survival curves of the 7 m7G-related lncRNAs model in the train, test, and entire sets. (a–c) Kaplan–Meier curves of OS of patients between low- and high-risk groups in the train, test, and whole groups. (d) Kaplan–Meier curves of OS stratified by age, gender, and stage between low-/high-risk groups in the whole groups.

immunotherapy and then further forecast the immunotherapeutic advantages of the risk model. In this predictive model, individuals with low-risk score had a higher IPS-CTLA4-negtive-PD1-negtive score and an IPS-CTLA4-positive-PD1-negtive score ($p < 0.05$; Fig. 9c), implying that they were more likely benefit from immunotherapy.

3.5. Distinguishing BLCA clusters and prediction of immunotherapy

According to previous study, different clusters usually represented distinct immune microenvironments, which resulted in various immunotherapeutic effects [25,26]. Based on the expression of seven m7G-related lncRNAs, we separated patients into two groups using the ConsensusClusterPlus (CC) R package (Fig. 8a). We found that patients in cluster 1 had longer OS ($p = 0.002$) in the Kaplan–Meier curve (Fig. 8b). Furthermore, the association between 2 risk groups and 2 clusters was presented in Sankey diagram (Fig. 8c). Additionally, T-distributed stochastic neighbor embedding (t-SNE) was utilized to elucidate that two risk groups and two clusters can be clearly discriminated with precision (Fig. 8d). Additionally, PCA were used to confirm that both two clusters and risk subgroups possess distinct PCA (Fig. 8e).

Cluster 2 had a higher concentration of immune cells than Cluster 1 on the basis of the examination of tumor-infiltrating immune cells in different platforms (Fig. 8h). Differential expression analysis expressions of immune checkpoint gene suggested that 30 of 47 genes were increased significantly in Cluster 2 than in Cluster 1, such as CTLA4, CD80, CD86, CD274 (PD-L1), PDCD1 (PD-1), and PDCD1LG2 (PD-L2) (Fig. 8f). Moreover, compared to Cluster 2, Cluster 1 displayed a lower immunological score and a lower ESTIMATE score, representing a distinct TME (Fig. 8g).

To further predict the response of immunotherapy, TIDE score and IPS score were calculated between two clusters. There was no remarkable distinction between the two clusters in TIDE score, MSI score, T-cell dysfunction score and T-cell exclusion score (Fig. 9b). Cluster 1 had a greater IPS-CTLA4-negative-PD1-negative score, while Cluster 2 had higher IPS-CTLA4-negative-PD1-positive score and higher IPS-CTLA4-positive-PD1-positive score (Fig. 9d). Above results may indicate that immunotherapy may be more effective for Cluster 2.
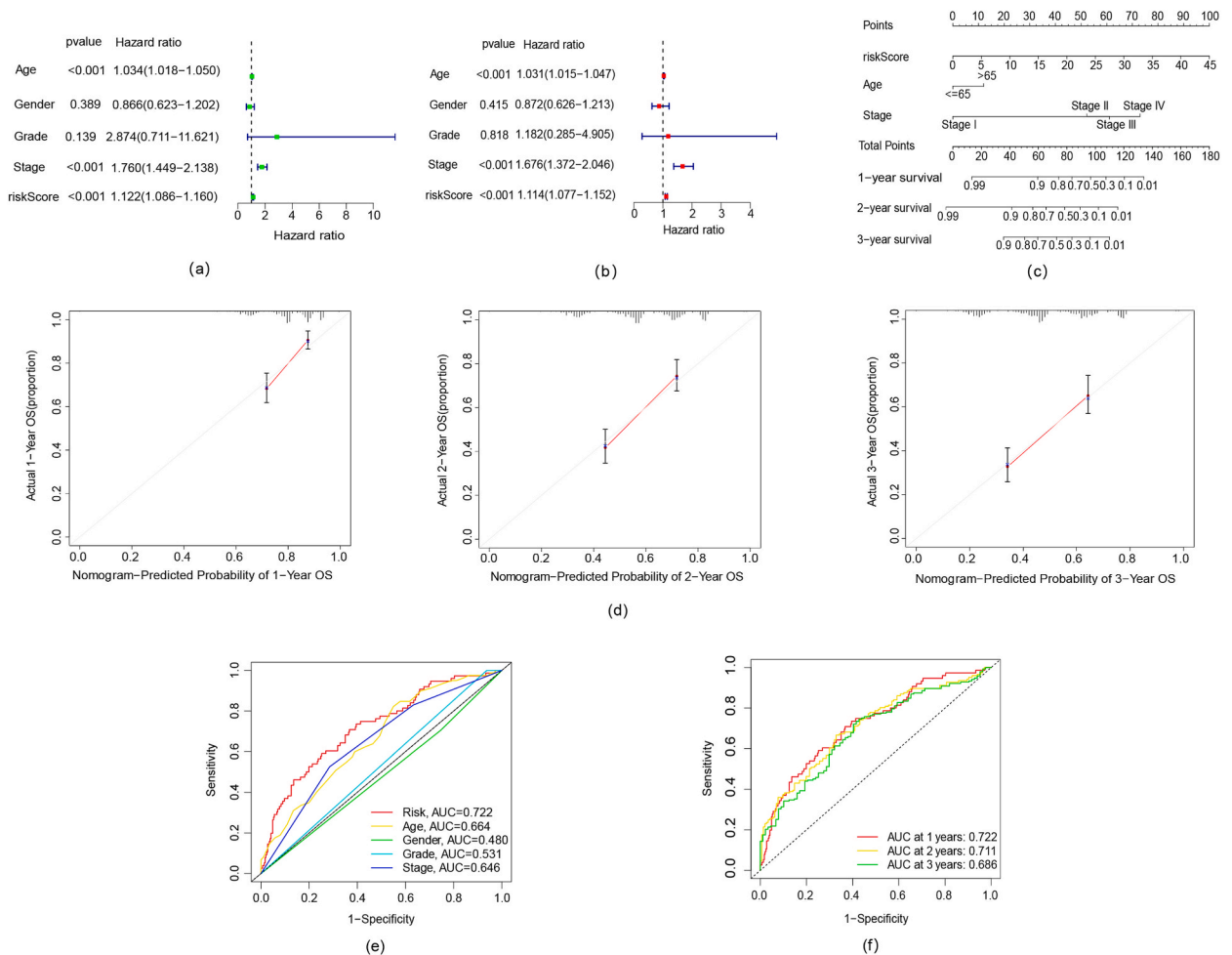
Fig. 6. Nomogram and evaluation of the prognosis model. (a, b) Uni- and multi-Cox regression of clinical characteristics and risk score with OS. (c) The nomogram constructed by risk score, age, and stage. (d)The calibration curves for 1-, 2-, and 3-year OS. (e) The 1-year ROC curves of clinical variables and risk score. (f) The 1-, 2-, and 3-year ROC curves of the whole group.

4. Discussion

Although lncRNA and m7G modification have been studied that they had the indispensable roles in carcinogenesis and immu-notherapy [22,27], it still remains uncertain whether the m7G-lncRNAs contributes to the development of bladder cancer. Thus, in our research, we discovered m7G-related lncRNAs and established a seven m7G-related lncRNA model that was remarkably related with overall survival for the first time. Then, the BLCA patients were split into low- and high-risk subgroups, and the differences between the two groups were further examined using IPS, TICs, TME, TIDE, and survival analysis. We anticipate that this model will facilitate the improvement of individualized treatment options for BLCA.

Previous researches have indicated that the METTL1-mediated m7G tRNA modifications were related with a malignant subtype in many diseases, including cancer [14,28,29]. Furthermore, cancers include intrahepatic cholangiocarcinoma and lung cancer have higher levels of METTL1, which was associated to worse survival [30,31]. Nevertheless, it has not been observed how m7G-associated lncRNAs affect BLCA patients' survival. Employing reliable biological analysis, our study initially isolated 29 genes closely related to m7G before identifying 7 prognostic lncRNAs for the prognosis model. AC073534.2, NRIR, UBE2Q1-AS1, and AC253576.2 were determined as protective variables, while AC093620.1, KCNQ1OT1, and AC083906.3 were determined as risk factors. Moreover, of the seven lncRNAs, several have been reported to have biological effects. For instance, KCNQ1OT1 can affect miR-218-5p/HS3ST3B1 to promote bladder cancer migration and invasion [32]. A possible biomarker for the early-stage diagnosis of colorectal cancer was the serum exosomal NRIR, which was considerably increased in colorectal cancer [33]. Then, we developed a prognostic model containing 7 lncRNAs. According to the prognostic model, we separated BLCA patients into low- and high-risk groups; in TCGA data, patients in the high-risk category have a shorter survival rate. To assess the reliability of the prognostic signature, we used the ROC curve, Kaplan-Meier curve, and survival status distribution. Furthermore, risk score was shown to be a highly accurate predictor of overall survival in BLCA, as shown by the 1-2- and 3-year nomograms. The calibration curves further demonstrated the model's precision.
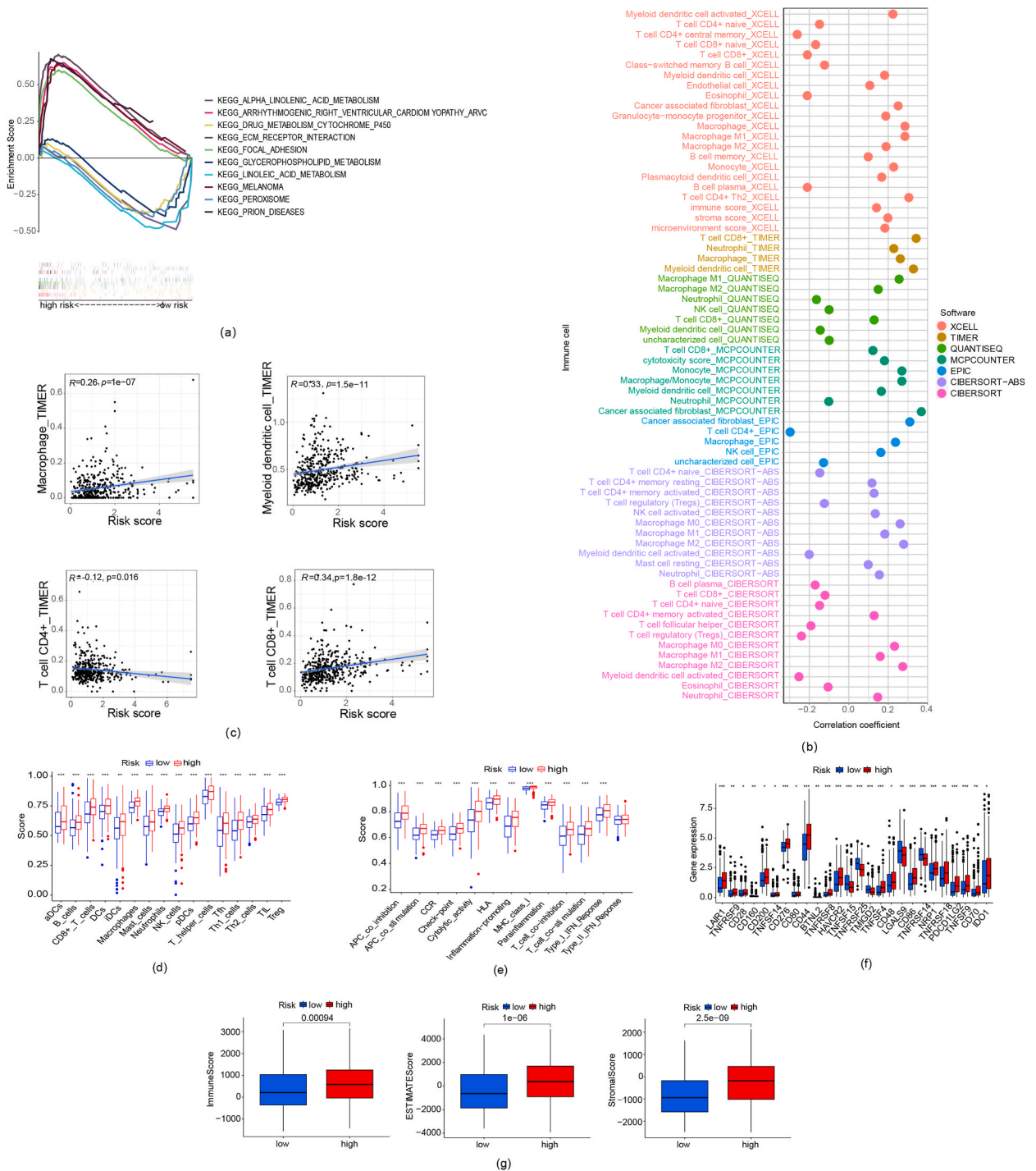
Fig. 7. The analysis of immune cells, immune checkpoint and tumor microenvironment. (a) GSEA of the top 5 pathways enriched in two risk group. (b)The immune cell bubble of risk groups. (c)The association between risk score and immune cells. (d) Difference of infiltrating immune cell subgroups and levels between low-/high-risk groups. (e) Difference of enrichment of immune-associated signatures between low-/high-risk groups. (f) Difference of checkpoints expression between low-/high-risk groups. The expression level of (d–f) were compared by the Wilcoxon test (*, P < 0.05; **, P < 0.01, ***P < 0.001). (g) Difference of immune-related scores between low-/high-risk groups.

GSEA showed melanoma, prion-diseases, ECM-receptor-interaction, arrhythmogenic-right-ventricular-cardiomyopathy-arvc, focal-adhesion were the top five enriched pathways in high-risk subgroups. KEGG_MELANOMA was a KEGG pathway containing 71 genes that were associated with the melanoma development pathway [34]. The Ras-Raf-MEK-ERK and PI3K-AKT signaling
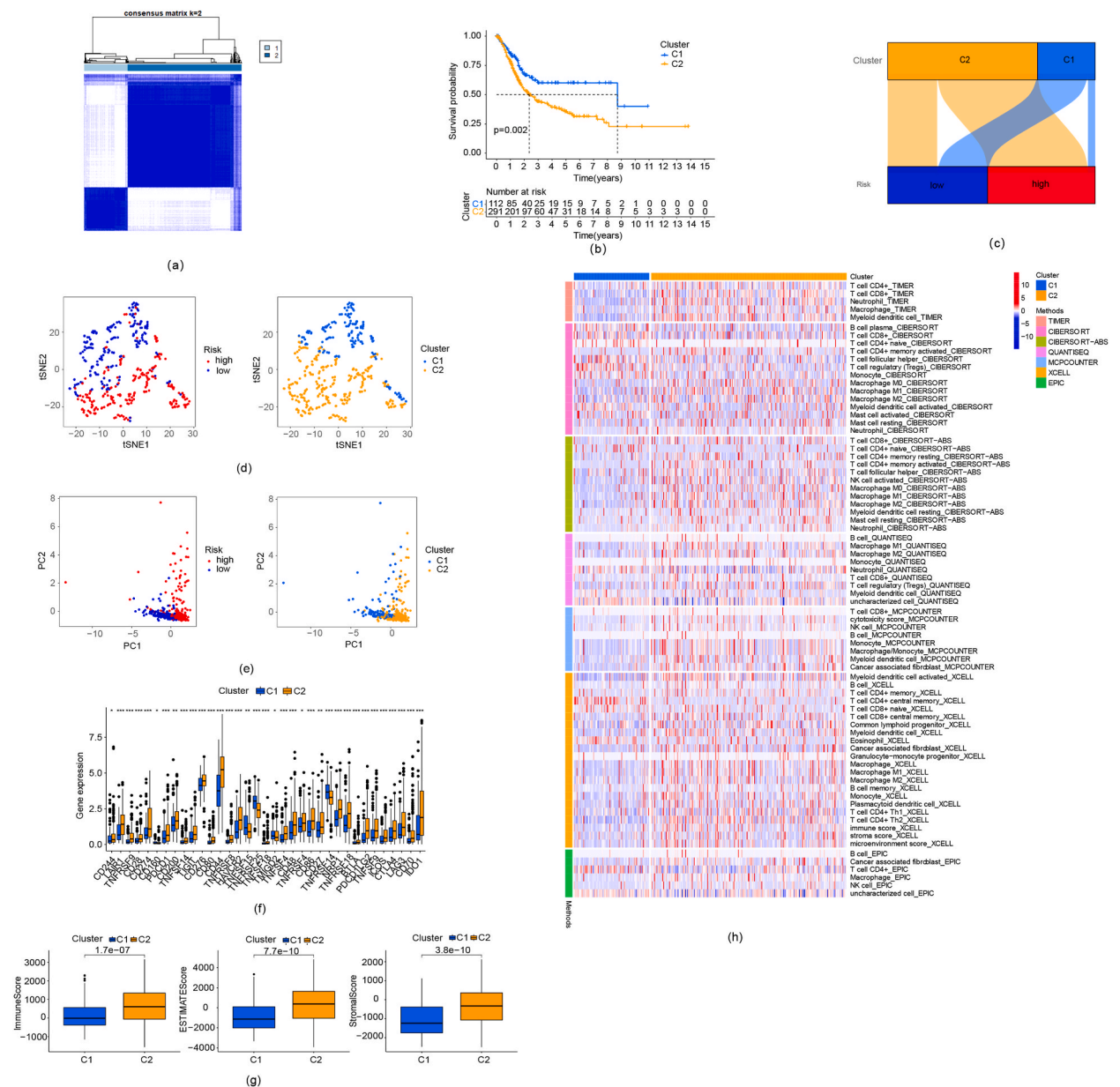
Fig. 8. Differences between two clusters. (a) Patients divided into two clusters by ConsensusClusterPlus. (b) Kaplan–Meier survival curves of OS in two clusters. (c) Sankey diagram between risk groups and clusters. (d) t-SNE of risk groups and clusters. (e) PCA of risk groups and clusters. (f) The heatmap of immune cells in two clusters. (g) Difference of checkpoints expression in two clusters. The expression level were compared by the Wilcoxon test (*, $P < 0.05$; **, $P < 0.01$, ***$P < 0.001$). (h) Difference of immune-related scores between two clusters.

pathways were both important effector pathways which played a vital role in melanoma progression [35]. Besides, by controlling tumor cell proliferation, migration, invasion, and drug tolerance, overactivation of the PI3K/AKT pathway encouraged the tumor progression of cells [36–38], while suppression of the PI3K/AKT pathway can stop bladder cancer cells from proliferating and growing [39]. Similarly, it has been reported that Ras-Raf-MEK-ERK was activated in bladder cancer cells [40] and collaborates with Wnt signaling in development of urothelial cell carcinoma [41]. KEGG_PRION_DISEASES contained mechanisms that may lead to neuronal death, such as oxidative stress, regulated activation of complement, and endoplasmic reticulum stress. Several studies have reported that bladder cancer patients had increased levels of oxidative stress [42], and bladder cancer extracellular vesicles can promote the tumor growth, metastasis, and recurrence by stimulating unfolded protein response during endoplasmic reticulum stress [43]. Extracellular matrix (ECM) was one of the most prevalent elements of the tumor microenvironment. Furthermore, ECM concentration in tumors serves as a barrier to impede the effects of therapy on tumor cells [44]. It has been also investigated that ECM-related genes were related with poor prognosis and tumor recurrence of bladder cancer [45]. Currently, association between
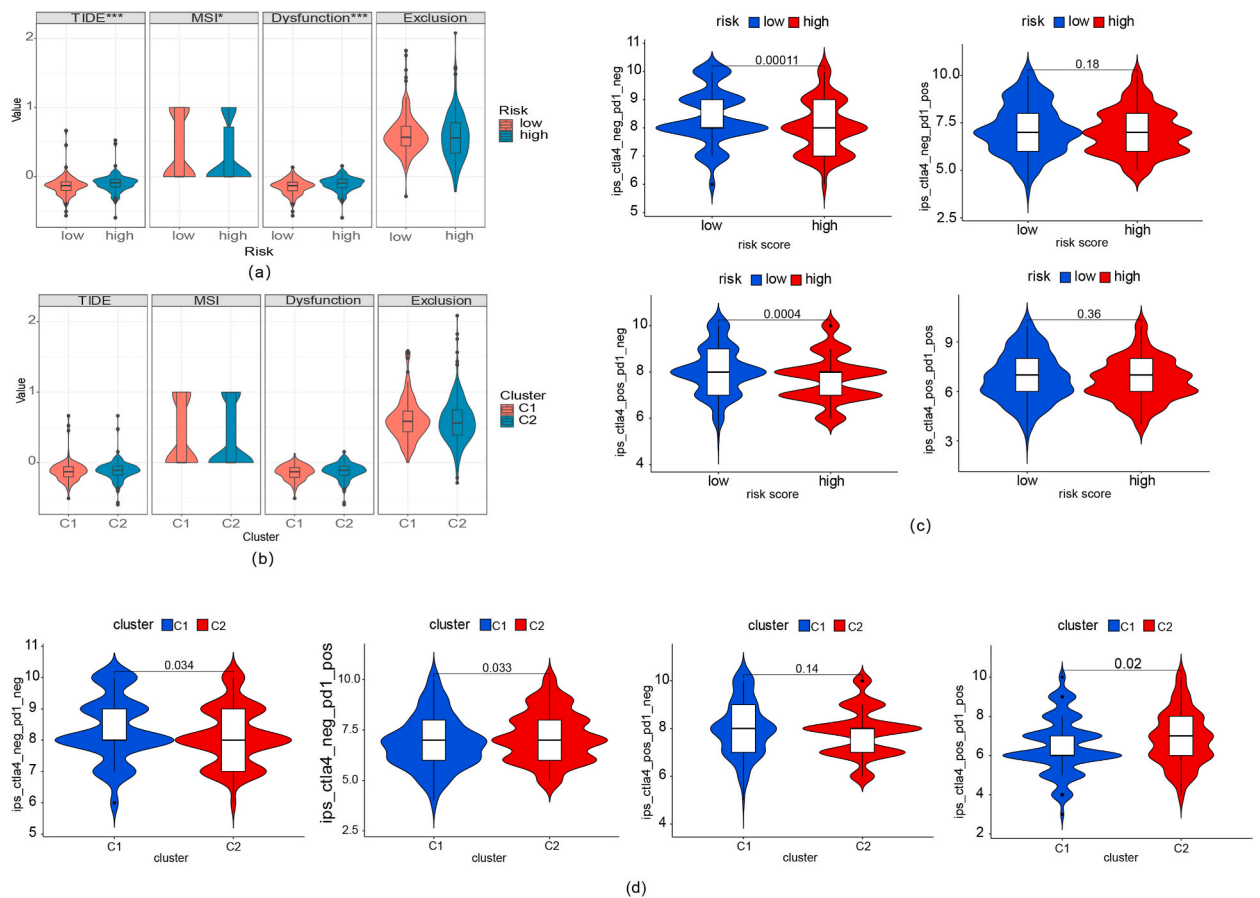
Fig. 9. Immunotherapy prediction of risk groups and clusters. (a–b) TIDE, MSI, and T-cell exclusion and dysfunction score in risk groups and clusters. The scores were compared by the Wilcoxon test (ns, not significant; *, P < 0.05; **, P < 0.01, ***P < 0.001). (c) IPS, IPS-PD1-positive, IPS-CTLA4-positive, and IPS-PD1-CTLA4-positive score distribution plot in risk groups. (d) IPS, IPS-PD1-positive, IPS-CTLA4-positive, and IPS-PD1-CTLA4-positive score distribution plot in clusters.

KEGG_ARRHYTHMOGENIC_RIGHT_VENTRICULAR_CARDIOMYOPATHY_ARVC pathway and bladder cancer has not been reported, which will be one of our future research directions. In addition, structural molecules associated with focal adhesion were investigated for their ability to regulate tumor cell epithelial mesenchymal transition (EMT) and promote tumor invasion and metastasis [46]. Focal adhesion kinase (FAK) was found to be engaged in adjusting bladder cancer's invasion and migration [47].

All immune cells, including neutrophils, macrophages, $CD8^+$ T cells, NK cells, and others, were considerably higher in the high-risk group, according to the ssGSEA data. According to specific research, the rate of tumor immune cell infiltration is connected to the prognosis of cancer patients. For instance, TIGIT + $CD8^+$ T-cells was a poor prognostic indicator of survival for muscle invasive bladder cancer [48]. A high ratio of neutrophils to lymphocytes was a valuable predictor for the worse OS in BLCA patients [49]. Furthermore, meaningful upregulation of immune-associated pathways was also observed in the high-risk group. That is to say, despite having enhanced immunological activity, high-risk group may have suppressed anti-tumor immunity, which explained their poor survival. This also provides a fresh perspective on bladder cancer immunotherapy. BLCA has been found to be particularly responsive to immunotherapy because of its high mutational burden in recent years [50–52]. Yet, the immunotherapy benefit was still confined to a subset of patients, and research findings varied [51,53]. Consequently, we analyzed immune checkpoint expression, TIDE score, and IPS score in two risk groups and clusters in an effort to identify a new biomarker for bladder cancer immunotherapy. We elucidated that most of ICB genes were elevated in Cluster 2 and high-risk group. However, combining IPS and TIDE analysis, cluster 2 patients and those in the low-risk group may benefit more from immunotherapy, which may result from the higher expression of CTLA4, CD274, and PDCD1 in Cluster 2. We anticipate that the aforementioned research will create a new method of accurate and personalized therapy for BLCA patients.

Our study has several shortcomings. Firstly, a larger sample is essential to validate the prognostic model. Secondly, except for experimental evidence of KCNQ1OT1 [32], there are few investigations for the role of the other 6 lncRNAs in BLCA. To investigate the precise mechanism by which our discovered m7G-related lncRNAs affect bladder cancer, more experimental verification is required. Furthermore, our analyses were employed based on public databases, and all data were collected retrospectively. Therefore, the outcomes may be affected by selection bias. Large prospective researches are also needed to verify our result.

5. Conclusions

M7G-related lncRNAs could forecast overall survival of bladder cancer and immunotherapy response, thereby advancing personalized treatment. The mechanisms among m7G, immunity, lncRNAs, and bladder cancer were deserved exploring and studying in future research.

Ethics approval and informed consent

According to the Declaration of Helsinki, the current study was approved by the Ethics Committee of The Second Affiliated Hospital and Yuying children's Hospital of Wenzhou Medical University. Since our study only collected information from the TCGA database, written informed consent was not required.

Funding

No funding received.

Data availability

You can get the data used to support our findings at the TCGA (https://portal.gdc.cancer.gov), GSEA (http://www.gsea-msigdb.org/gsea/index.jsp).

Authors' contributions

(I) Conceived and designed the experiments: All authors (II) Performed the experiments: Shangxun Xie, Baofu Feng, Dapang Rao, Shuaibin Wang (III) Analyzed and interpreted the data: Shangxun Xie, Jibao He(IV) Contributed reagents, materials, analysis tools or data: Shangxun Xie, Jibao He, Youhua He (V) Wrote the paper: All authors.

Supplementary Information

Appendix Table S1: the table of m7G-related genes refers to GSEA (gene sets M26714, M26066, and M18244) and previous studies. Appendix Table S2: the network information of m7G-related genes and lncRNAs. Appendix Table S3: profile of significantly dysregulated immune cells between two risk groups in several platforms.

Appendix C. Supplementary data

Supplementary data related to this article can be found at https://doi.org/10.1016/j.heliyon.2023.e15897.

References

[1] F. Bray, et al., Global cancer statistics 2018: GLOBOCAN estimates of incidence and mortality worldwide for 36 cancers in 185 countries, CA A Cancer J. Clin. 68 (6) (2018) 394–424.
[2] A.T. Lenis, et al., Bladder cancer: a review, JAMA 324 (19) (2020) 1980–1991.
[3] L.B. Alexandrov, et al., Signatures of mutational processes in human cancer, Nature 500 (7463) (2013) 415–421.
[4] N.M. Donin, et al., Immunotherapy for the treatment of urothelial carcinoma, J. Urol. 197 (1) (2017) 14–22.
[5] Y.M. Ning, et al., FDA approval summary: atezolizumab for the treatment of patients with progressive advanced urothelial carcinoma after platinum-containing chemotherapy, Oncol. 22 (6) (2017) 743–749.
[6] J. Bellmunt, et al., Pembrolizumab as second-line therapy for advanced urothelial carcinoma, N. Engl. J. Med. 376 (11) (2017) 1015–1026.
[7] P. Boccaletto, et al., RNArchitecture: a database and a classification system of RNA families, with a focus on structural information, Nucleic Acids Res. 46 (D1) (2018) D202–d205.
[8] P. Boccaletto, et al., MODOMICS: a database of RNA modification pathways. 2017 update, Nucleic Acids Res. 46 (D1) (2018) D303–d307.
[9] H.J. Chou, et al., Transcriptome-wide analysis of roles for tRNA modifications in translational regulation, Mol. Cell 68 (5) (2017) 978–992.e4.
[10] F. Liu, et al., ALKBH1-Mediated tRNA demethylation regulates translation, Cell 167 (3) (2016) 816–828.e16.
[11] F. Jühling, et al., tRNAdb 2009: compilation of tRNA sequences and tRNA genes, Nucleic Acids Res. 37 (2009) D159–D162 (Database issue).
[12] A. Alexandrov, M.R. Martzen, E.M. Phizicky, Two proteins that form a complex are required for 7-methylguanosine modification of yeast tRNA, RNA 8 (10) (2002) 1253–1266.
[13] L. Pandolfini, et al., METTL1 promotes let-7 MicroRNA processing via m7G methylation, Mol. Cell 74 (6) (2019) 1278–1290.e9.
[14] Y. Liu, et al., Methyltransferase-like 1 (METTL1) served as a tumor suppressor in colon cancer by activating 7-methyguanosine (m7G) regulated let-7e miRNA/HMGA2 axis, Life Sci. 249 (2020), 117480.
[15] X. Ying, et al., METTL1-m(7) G-EGFR/EFEMP1 axis promotes the bladder cancer development, Clin. Transl. Med. 11 (12) (2021) e675.
[16] Y. Fang, M.J. Fullwood, Roles, functions, and mechanisms of long non-coding RNAs in cancer, Dev. Reprod. Biol. 14 (1) (2016) 42–54.
[17] L. Statello, et al., Gene regulation by long non-coding RNAs and its biological functions, Nat. Rev. Mol. Cell Biol. 22 (2) (2021) 96–118.
[18] Y.J. Yan, et al., Comprehensive characterization of common and cancer-specific differently expressed lncRNAs in urologic cancers, Comput. Math. Methods Med. 2021 (2021), 5515218.
[19] H. Luo, et al., lncRNA CASC11 promotes cancer cell proliferation in bladder cancer through miRNA-150, J. Cell. Biochem. 120 (8) (2019) 13487–13493.

[20] C. Chen, et al., Exosomal long noncoding RNA LNMAT2 promotes lymphatic metastasis in bladder cancer, J. Clin. Invest. 130 (1) (2020) 404–421.

[21] M. Machitani, I. Taniguchi, M. Ohno, ARS2 regulates nuclear paraspeckle formation through 3'-end processing and stability of NEAT1 long noncoding RNA, Mol. Cell Biol. 40 (4) (2020).

[22] G. Shan, et al., Long non-coding RNA NEAT1 promotes bladder progression through regulating miR-410 mediated HMGB1, Biomed. Pharmacother. 121 (2020), 109248.

[23] C. Tomikawa, 7-Methylguanosine modifications in transfer RNA (tRNA), Int. J. Mol. Sci. 19 (12) (2018).

[24] A. Goodman, S.P. Patel, R. Kurzrock, PD-1-PD-L1 immune-checkpoint blockade in B-cell lymphomas, Nat. Rev. Clin. Oncol. 14 (4) (2017) 203–220.

[25] R.J. DeBerardinis, Tumor microenvironment, metabolism, and immunotherapy, N. Engl. J. Med. 382 (9) (2020) 869–871.

[26] S. Das, K. Camphausen, U. Shankavaram, Cancer-specific immune prognostic signature in solid tumors and its relation to immune checkpoint therapies, Cancers 12 (9) (2020).

[27] Z. Gao, et al., A comprehensive analysis of METTL1 to immunity and stemness in pan-cancer, Front. Immunol. 13 (2022), 795240.

[28] Q.H. Tian, et al., METTL1 overexpression is correlated with poor prognosis and promotes hepatocellular carcinoma via PTEN, J. Mol. Med. (Berl.) 97 (11) (2019) 1535–1545.

[29] S. Lin, et al., Mettl1/Wdr4-Mediated m(7)G tRNA methylome is required for normal mRNA translation and embryonic stem cell self-renewal and differentiation, Mol. Cell 71 (2) (2018) 244–255.e5.

[30] Z. Dai, et al., N(7)-Methylguanosine tRNA modification enhances oncogenic mRNA translation and promotes intrahepatic cholangiocarcinoma progression, Mol. Cell 81 (16) (2021) 3339–3355.e8.

[31] J. Ma, et al., METTL1/WDR4-mediated m(7)G tRNA modifications and m(7)G codon usage promote mRNA translation and lung cancer progression, Mol. Ther. 29 (12) (2021) 3422–3435.

[32] Y. Li, et al., LncRNA KCNQ1OT1 facilitates the progression of bladder cancer by targeting MiR-218-5p/HS3ST3B1, Cancer Gene Ther. 28 (3–4) (2021) 212–220.

[33] M. Yu, et al., Circulating serum exosomal long non-coding RNAs FOXD2-AS1, NRIR, and XLOC_009459 as diagnostic biomarkers for colorectal cancer, Front. Oncol. 11 (2021), 618967.

[34] M. Kanehisa, et al., KEGG for representation and analysis of molecular networks involving diseases and drugs, Nucleic Acids Res. 38 (2010) D355–D360.

[35] F. Meier, et al., The RAS/RAF/MEK/ERK and PI3K/AKT signaling pathways present molecular targets for the effective treatment of advanced melanoma, Front. Biosci. 10 (2005) 2986–3001.

[36] M.C. De Santis, et al., PI3K signaling in tissue hyper-proliferation: from overgrowth syndromes to kidney cysts, Cancers 9 (4) (2017).

[37] D. Li, et al., CADM2, as a new target of miR-10b, promotes tumor metastasis through FAK/AKT pathway in hepatocellular carcinoma, J. Exp. Clin. Cancer Res. 37 (1) (2018) 46.

[38] D.J. Mulholland, et al., Pten loss and RAS/MAPK activation cooperate to promote EMT and metastasis initiated from prostate cancer stem/progenitor cells, Cancer Res. 72 (7) (2012) 1878–1889.

[39] W.L. Li, et al., Purple sweet potato anthocyanin exerts antitumor effect in bladder cancer, Oncol. Rep. 40 (1) (2018) 73–82.

[40] I. Boulalas, et al., Activation of RAS family genes in urothelial carcinoma, J. Urol. 181 (5) (2009) 2312–2319.

[41] I. Ahmad, et al., Ras mutation cooperates with β-catenin activation to drive bladder tumourigenesis, Cell Death Dis. 2 (3) (2011) e124.

[42] H. Pelicano, D. Carney, P. Huang, ROS stress in cancer cells and therapeutic implications, Drug Resist. Updates 7 (2) (2004) 97–110.

[43] C.H. Wu, et al., Bladder cancer extracellular vesicles drive tumorigenesis by inducing the unfolded protein response in endoplasmic reticulum of nonmalignant cells, J. Biol. Chem. 294 (9) (2019) 3207–3218.

[44] E. Henke, R. Nandigama, S. Ergün, Extracellular matrix in the tumor microenvironment and its impact on cancer therapy, Front. Mol. Biosci. 6 (2019) 160.

[45] H. Zhao, et al., Prediction of prognosis and recurrence of bladder cancer by ECM-related genes, J Immunol Res 2022 (2022), 1793005.

[46] I. Akrida, et al., Expression of EMT inducers integrin-linked kinase (ILK) and ZEB1 in phyllodes breast tumors is associated with aggressive phenotype, Histol. Histopathol. 33 (9) (2018) 937–949.

[47] D.B. Kong, F. Chen, N. Sima, Focal adhesion kinases crucially regulate TGFβ-induced migration and invasion of bladder cancer cells via Src kinase and E-cadherin, OncoTargets Ther. 10 (2017) 1783–1792.

[48] Z. Liu, et al., Intratumoral TIGIT(+) CD8(+) T-cell infiltration determines poor prognosis and immune evasion in patients with muscle-invasive bladder cancer, J Immunother Cancer 8 (2) (2020).

[49] Y.G. Tan, et al., High neutrophil-to-lymphocyte ratio predicts worse overall survival in patients with advanced/metastatic urothelial bladder cancer, Int. J. Urol. 25 (3) (2018) 232–238.

[50] M.S. Lawrence, et al., Mutational heterogeneity in cancer and the search for new cancer-associated genes, Nature 499 (7457) (2013) 214–218.

[51] A. Necchi, et al., Pembrolizumab as neoadjuvant therapy before radical cystectomy in patients with muscle-invasive urothelial bladder carcinoma (PURE-01): an open-label, single-arm, phase II study, J. Clin. Oncol. 36 (34) (2018) 3353–3360.

[52] T. Powles, et al., Atezolizumab versus chemotherapy in patients with platinum-treated locally advanced or metastatic urothelial carcinoma (IMvigor211): a multicentre, open-label, phase 3 randomised controlled trial, Lancet 391 (10122) (2018) 748–757.

[53] T. Powles, et al., Clinical efficacy and biomarker analysis of neoadjuvant atezolizumab in operable urothelial carcinoma in the ABACUS trial, Nat. Med. 25 (11) (2019) 1706–1714.